

On the Aggregate Interference in Random CSMA/CA Networks: A Stochastic Geometry Approach

June Hwang, Jinho Choi, Riku Jäntti and Seong-Lyun Kim

Abstract

In this paper, we investigate the cumulative distribution function (CDF) of the aggregate interference in carrier sensing multiple access/collision avoidance (CSMA/CA) networks measured at an arbitrary time and position. We assume that nodes are deployed in an infinite two-dimensional plane by the Poisson point process (PPP) and that the channel model follows the singular path loss function and Rayleigh fading. To find the effective active node density we analyze the distributed coordinate function (DCF) dynamics in a common sensing area and obtain the steady-state power distribution within a spatial disk of radius $R/2$, where R is the effective carrier sensing distance. The results of a massive simulation using Network Simulator-2 (NS-2) show a high correlation with the derived CDF.

Index Terms

Aggregate interference, CSMA/CA, DCF, Poisson point process, NS-2

I. INTRODUCTION

A. Motivations

Due to the inherent scarcity of frequency spectrum and increasing wireless traffic demands, frequency reuse has become an essential key technological issue associated with contemporary wireless communication systems. Frequency reuse intrinsically causes interference between wireless links in both homogeneous and heterogeneous systems using the same frequency. Accordingly, the state of the aggregate interference

J. Hwang is with Samsung Electronics, Digital Media Center, Suwon, Korea. Email: june77.hwang@samsung.com. J. Choi is with the Department of Electrical and Electronic Engineering, Yonsei University, 50 Yonsei-Ro, Seodaemun-Gu, Seoul 120-749, Korea. Email: jhchoi@ramo.yonsei.ac.kr. R. Jäntti is with the Department of Communications and Networking, School of Electrical Engineering, Aalto University, P.O. Box 13000, FI-00076 Aalto, Finland. Email: riku.jantti@aalto.fi. S.-L. Kim is with the Department of Electrical and Electronic Engineering, Yonsei University, 50 Yonsei-Ro, Seodaemun-Gu, Seoul 120-749, Korea. Email: slkim@yonsei.ac.kr.

at an arbitrary position in the random node topology has become of great importance. Currently, unlicensed spectrum is considered to be a supplementary spectrum of Long Term Evolution (LTE) in the license-assisted access (LAA) system in the 3rd Generation Partnership Project (3GPP) [1]. For the system, the main incumbent networks at 5GHz are wireless local area networks (WLANs) which are based on IEEE 802.11 a/n/ac technologies. Because of the widespread deployment of WLAN systems, initiation of LTE operation in the unlicensed spectrum must be done carefully. In this context, it is necessary to understand the characteristics of the aggregate interference of IEEE 802.11 networks in order to design the operation rules of the LAA system. Furthermore, the interference can be controlled using the relationships discovered among the protocol parameters. Such control is useful in optimizing the operation of densely deployed WLAN and to protect incumbent systems against WLAN interference for cases in which the system shares spectrum [2], [3].

In this paper, we are interested in the aggregate interference of random carrier sense multiple access/collision avoidance (CSMA/CA) networks that are based on the IEEE 802.11 distributed coordination function (DCF). To the best of our knowledge, there has been no massive test at the simulator level for the aggregate interference of CSMA/CA networks. We test and analyze the interference at the protocol level, which reflects the contention and signaling processes of DCF. Consequently, the goal is to obtain the statistical inference of the aggregate interference and to verify the results via simulations. Our analysis tool is the stochastic geometry [4], [5].

To utilize the characteristics of aggregate interference in practical cases like those mentioned above, we would like to find the aggregate interference distribution in practical CSMA/CA networks, not an ideal CSMA network. Modeling a practical network requires a hybrid method that considers the both dependent and independent point processes together. The reason and the explanation are addressed in Section II. To capture the collision and idle time effects caused by imperfect contention of the real-life CSMA/CA operation, we propose modeling the system using the Poisson Point Process (PPP) with the *modified active node density*.

B. Previous works

Previous research has dealt with random CSMA networks. In [6] and [7], the authors derive the optimal carrier sense threshold in a CSMA/CA network. They directly adopt the Matérn approximation on active node density without verifying the validity of using this approximation for a realistic network situation. In [8], the authors derive an optimal spatial reuse of frequency for the CDMA system and prove that the

resulting guard zone gives better performance than ALOHA and CSMA. In [9], the authors propose a two phase slot system (using the backoff probability) and consider the directional antenna for the performance measurement. These two studies concluded that a CSMA network can work well and that optimized MAC parameters (the guard zone in [8], and the pathloss exponent, SNR and backoff probability in [9]) make the CSMA as an optimal scheme in the various multiple access methods. However, their assumptions, such as ideal CSMA operation and a Gaussian distribution of the aggregate interference (in [8]) or a PPP distribution of *winning transmitters* (in [9]) show that the considerations for practical MAC operation are insufficient. The main reason for these assumptions as described in [9] is that it is extremely complex to model the MAC layer operation details, since the practical CSMA/CA modeling is not snapshot-based; rather, it is based on the time and history of the MAC status. Therefore, the peculiarities of the CSMA/CA protocol, such as unnecessary waiting due to backoff and carrier sensing based contention, should be investigated further to justify the results.

Because of the complexity, most of the previous work has focused on ALOHA-like systems in which the aggregate interference can be analyzed by assuming that the transmitting nodes have independent locations and behaviors [10], [11]. Although broadband cellular systems such as LTE, LTE-A, WCDMA or its small cell networks can also be modeled using this independence, this is not a realistic assumption for CSMA/CA networks. In a network of CSMA/CA nodes, every communication entity first senses the ongoing transmission in the channel and then determines when to start transmitting. Consequently, transmission by a node will impact on its neighbors' channel access.

Our aim is to derive a PPP-based model for the aggregate interference of practical CSMA/CA networks. To reflect the real situation, we derive a new active node density considering DCF dynamics, collisions, etc. With the exception of [6], none of the aforementioned studies showed the results from the protocol-level simulation. Compared with these previous research efforts, our work investigates the exact distribution of aggregate interference in CSMA/CA networks and validates it by means of massive simulations using a known simulator.

C. Summary of contributions and organization of this paper

Our paper has the following notable results:

- **Because of the possibility of concurrent transmission within an exclusion area incurred through DCF operation, CSMA/CA random networks can be modeled by a hybrid point process combining independent and dependent processes (Section II).**

- **The effective node density reflecting CSMA/CA MAC layer operation is derived in Section III.**
- **The dominant factor of the derived effective node density is the carrier sensing range in the low initial node density regime and the other MAC parameters (data packet size and transmission mode) in the high initial node density regime (Section III).**
- **The aggregate interference using our derived effective node density is verified using the NS-2 network simulator and MATLAB simulations in Section IV.**
- **Contrary to the research assumptions made so far, the distribution of the CSMA/CA aggregate interference is neither normal nor log-normal distribution, where the higher the mean of the aggregate power, the lower the probability of that mean value (Section IV).**

II. POINT PROCESS FOR MODELING RANDOM CSMA/CA NETWORKS

In this section, we focus on determining which type of point process is suitable for modeling CSMA/CA networks. A generic wireless network consisting of multiple randomly deployed nodes can be described via a point process. In the point process, a mark (a scalar or a vector) can be assigned to each point independently, which is useful for modeling node-oriented properties such as the transmission power, medium access delay, etc. In particular, the case in which the number of nodes in a network is Poisson-distributed and their positions at a given time instant are independent of each other, is adequately explained by means of the PPP. The method to derive the aggregate power emitted from points at an arbitrary position under the independent marked PPP was previously studied as a *shot noise field*, which was originally used to model the noise in electronic circuits in the time domain.

A. Inappropriateness of PPP for CSMA/CA modeling

The PPP approach as it currently exists may be insufficient to model the CSMA/CA. The reason is that it does not reflect the carrier sensing philosophy. PPP is a typical *independent* point process in which the points are deployed independently of each other. On the other hand, in the carrier sensing operation, a sensing node always senses the shared medium and it delays its transmission once it senses that the medium is busy. The result is that active nodes are affected by each other, which means that the process is not independent.

B. Inappropriateness of the dependent point process

Let us now consider the dependent point process as a possible alternative. Here, the dependent point process means that some initially deployed points are discarded or selected by the metric relative to the other points' marks or locations. There are two dependent point processes that are most closely related to the modeling of CSMA/CA networks [10], [11]: the Matern hardcore (MHC) process and the simple sequential inhibition (SSI) point process. In [12], the authors are also motivated by the inappropriateness of PPP, i.e., the independence of points. In that paper, they compared the aggregate power distributions of PPP, MHC, and SSI with simulations, and concluded that SSI is most appropriate for modeling CSMA networks. However, their result is not fully acceptable because the operation they used in the simulation was not the real one, but a modified version of a dependent point process using IEEE 802.15.4 PHY parameters. They considered neither the details of practical MAC layer parameters nor the channel characteristics. A related paper [13] tries to solve the above issue by considering the backoff timer. However, there is still no consideration of the collision case, and the problem of underestimating the node intensity has not been fully solved.

MHC and SSI are fundamentally based on the hard exclusion area; nevertheless, they contain ambiguities in the determination of this area. Our simulation results further illustrate the issue. We simulated a realistic CSMA/CA network using NS-2 in order to observe the concurrent transmission behavior. Fig. 1 shows our simulation topology and the effect on the distribution of the number of concurrent transmitting nodes. In the grid topology, the black dot represents the transmitter where the corresponding receiver is located 5m to the right and 5m above its transmitter; the receiver is omitted from the figure. In the simulation, a 500 B payload is given to each transmitter and the traffic is saturated. The distance between the two nearest black dots is 50 (m), and the carrier sensing (CS) threshold is tuned so that the resulting CS range is 70 (m), as derived using Equation (6). All other parameters are the same as those in Table II. The larger circle, including the set C nodes in the center, denotes the CS area of the white dot (one of the transmitters), while the smaller circle, including the set B nodes, has a radius that is one half of the CS range. We depict the relative time durations on the number of concurrent transmissions in each set of the bar plot.

In the bar chart, two things are noteworthy: First, there is a time period in which two nodes are concurrently transmitting when all transmitters are even in each other's CS area (see Set B in the bar plot). Second, there is a time period in which the medium is idle in the full CS area (Set C). The first case

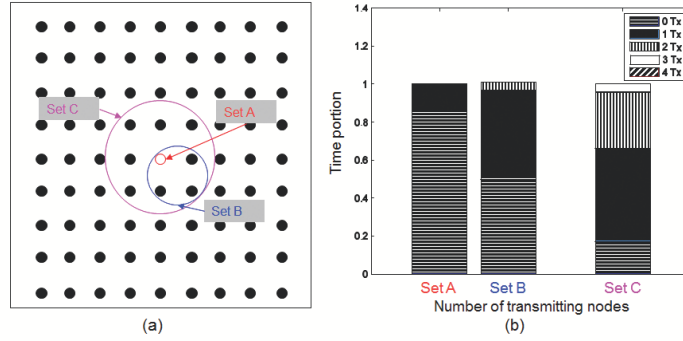


Fig. 1. The number of transmitting nodes concurrently: (a) scenario and (b) result.

occurs due to a CS failure or a collision in a real situation. MHC and SSI are fully *dependent thinning* of PPP with the exclusion area, and they cannot model these events. The resulting effective node density of the dependent point process is likely to be lower than that of the real one. These approaches may work well in collision-less CSMA/CA networks where the slot time is zero and the backoff time is a continuous random variable (including [14]), rather than in real situations. The second case occurs due to the idle time from the binary exponential backoff (BEB) and the distributed coordinate function. In the dependent point process, any point having none of the other points in its exclusion area always survives. The resulting effective node density of this process is likely to be higher than that of the real one. *As a result, the real operation of a CSMA/CA network has factors with both higher and lower effective node densities than that of the dependent point process.* This difference is due to the lack of MAC layer operation modeling in the dependent point process.

C. Revisit of PPP with a New Density

Collision events occur with a certain probability in real situations. This means that the concurrent transmission in an exclusion area occurs with some probability, not with deterministic patterns. This stochastic characteristic of real networks can be appropriately modeled using the independent point process. Therefore, we believe that a possible way to model a CSMA/CA network is again to use the independent PPP, but with a *new* effective active node density reflecting MAC layer operations. At the very least, the aggregate power at an arbitrary position can be elaborated more when using PPP with a new effective node density rather than pure PPP or MHC/SSI.

For our analysis, we consider an infinite plane where the transmitting nodes are deployed randomly at positions specified by a Poisson distribution with intensity λ . Each node transmits with a constant power p . The radio channel attenuates with the pass-loss exponent $\alpha = 4$ and Rayleigh fading. Then we have

the CDF and PDF, respectively, of the aggregate interference I at an arbitrary receiver as follows [7], [4]:

$$F_I(t) = \operatorname{erfc}\left(\frac{\lambda\pi^2\sqrt{p}}{4\sqrt{t}}\right), \quad (1)$$

$$f_I(t) = \frac{\exp\left(\frac{-\pi^4\lambda^2 p}{16t}\right)\pi^{3/2}\frac{\lambda}{p}}{4\left(\frac{t}{p}\right)^{3/2}}, \quad (2)$$

where $\operatorname{erfc}(x) = \frac{2}{\sqrt{\pi}} \int_x^\infty e^{-t^2} dt$ is a complementary error function.

Our idea is to use the above PDF and CDF again for calculating the aggregate interference of the CSMA/CA network, but with a new density λ' , which is called the *effective active node density* reflecting all of the CSMA parameters. Section III is devoted to describing how we obtain λ' , and its verification through massive NS-2 simulations is described in Section IV. Readers who are more interested in the results should go directly to Section IV.

III. EFFECTIVE ACTIVE NODE DENSITY

In this section, we obtain the effective active node density, which is defined as the average number of transmitting nodes per unit area. To derive the density, we first introduce the concept of a *mutual sensing area*. Then we derive the probability of a number of active nodes and the probability that a channel is busy in that area. At the end of this section, we obtain the effective active node density.

A. Effective carrier sensing range and mutual sensing area

Let us introduce a CS range R such that a sensing node can sense any ongoing transmission in this range. Then within a disk of radius $\frac{R}{2}$, every node senses each other. We set this disk as the mutual sensing area.

CS is based on the threshold γ , i.e., if the sensed power level at a sensing node is greater (or lower) than γ , a sensing node regards the channel as busy (or idle). The definition of R can be also interpreted as a minimum energy detection boundary. We assume that there is only one interferer near the sensing node. Then, the CS probability versus the distance to this interferer is calculated as follows:

$$\mathbb{P}[\text{Channel is busy}] = \mathbb{P}\left[\frac{p_i}{r^4} + \nu \geq \gamma\right], \quad (3)$$

where p_i is a random variable (RV) representing the product of the fading effect and the constant transmission power from a typical node i , r is the distance between the sensing node and the interferer,

and ν is the receiver noise power. Considering Rayleigh fading, p_i follows $\text{Exp}(1/p)$ with a constant transmission power p .

Consequently, with the CS range R , we convert the stochastic CS to a deterministic one. First, the average residual sensing area is calculated by integrating the parts of the circumference, of which the radius and the center are r and the sensing node, respectively. The CS probability of a point on this circumference is calculated using (3):

$$\begin{aligned} & \int_0^\infty 2\pi r \cdot \mathbb{P}\left[\frac{p_i}{r^4} + \nu \geq \gamma\right] dr \\ &= \int_0^\infty 2\pi r e^{-\frac{1}{p}(\gamma-\nu)r^4} dr \\ &= \frac{\pi^{3/2}}{2\sqrt{\frac{\gamma-\nu}{p}}} \end{aligned} \quad (4)$$

Assuming that the deterministic CS region should have the same average residual sensing area (sensing resolution) as the stochastic CS, the following equation is derived:

$$\frac{\pi^{3/2}}{2\sqrt{\frac{\gamma-\nu}{p}}} = \pi R^2 \quad (5)$$

Finally, we get the CS distance R as follows:

$$R = \frac{1}{\sqrt{2}} \left(\frac{\pi p}{\gamma - \nu} \right)^{1/4} \quad (6)$$

By using this deterministic CS distance, which we will call the *effective carrier sensing range*, the interference is regarded as Boolean at a given distance rather than stochastic.

Let us consider an infinite plane in which the nodes are randomly deployed. Assume that there is an arbitrary disk having a radius $R/2$ in the plane (mutual sensing area), where every node in this area can sense other nodes' transmissions according to the definition of the CS range R . By using the PPP, the number of deployed nodes in the mutual sensing area follows a Poisson distribution with the parameter $\lambda\pi(\frac{R}{2})^2$ as follows:

$$\mathbb{P}[N = n] = \frac{\{\lambda\pi(\frac{R}{2})^2\}^n}{n!} \exp\left(-\lambda\pi\left(\frac{R}{2}\right)^2\right) \quad (7)$$

Once we know $\mathbb{P}[N = n]$, we derive the probability of the number of active nodes, N_a , in the mutual sensing area $\mathbb{P}[N_a = a|N = n]$ and the power distribution at an arbitrary time instant in the mutual sensing area. These are explained in the following subsections. For the explanation, let us define the following

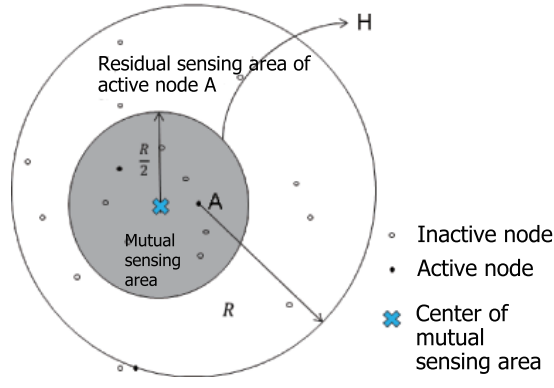


Fig. 2. If we pick up a certain mutual sensing area, every transmitting node in that area has its own residual sensing area. If there is no ongoing transmission in its residual sensing area, that node is the active node.

probability first:

Definition 1. p_{on} is the probability that there are ongoing transmissions in a given mutual sensing area at a certain time.

B. Number of active nodes, N_a in a mutual sensing area

Consider a given mutual sensing area H . Let the *residual sensing area* be defined as the sensing node's CS area, excluding H . (See the asymmetric donut in Fig. 2 for the relation between the sensing and mutual sensing areas.) The active node is defined here as the sensing node that has no ongoing transmissions in its residual sensing area. The CS results for each sensing node in H are random. Therefore, N_a is an RV that varies within $[0, N]$.

For a sensing node in H to be active, the CS result sensed from its residual sensing area must be idle, and that sensed from H must also be idle. We can find the distribution of N_a in H as in (8) when the probability p_{on} of Definition 1 is given:

$$\mathbb{P}[N_a = a | N = n] = \sum_{\eta=0}^8 P_{n,a,\eta} p_{\eta},$$

$$a = 0, \dots, n, \quad (8)$$

where

$$P_{n,a,\eta} = \binom{n}{a} \left(\frac{\eta}{8}\right)^a \left(1 - \frac{\eta}{8}\right)^{n-a}.$$

and

$$p_\eta = \sum_{D=0}^8 O_\eta^D p_{on}^D (1 - p_{on})^{8-D}. \quad (9)$$

A description of the detailed derivation of (8) is given in Appendix I.

C. Steady-state power distribution in a mutual sensing area

1) *DCF dynamics in a mutual sensing area*: Consider the IEEE 802.11 DCF protocol for CSMA/CA MAC. If all of the transmitting nodes can sense each other in a mutual sensing area and the given traffic to each node is saturated, we know the steady-state behavior in this area. As shown in [15] and subsequent research efforts, the backoff stage of each node in the network is random at a certain time, which can be elaborated through a two-dimensional Markov chain. We have two main quantities for addressing this: p_c is the probability that a collision happens conditioned on the transmission of each node, and τ is the transmission probability of a node at a randomly chosen time slot. These two quantities are derived by finding the steady-state solution of the discrete time Markov chain.

By following the notations of [7], we have the BEB dynamics with a maximum backoff stage m , a maximum retry limit $K (\geq m+2)$, and an initial window size W_0 . The probability τ that a node transmits in a randomly chosen time slot is:

$$\tau = \left\{ \frac{(1 - p_c)W_0(1 - (2p_c)^m)}{2(1 - p_c^K)(1 - 2p_c)} + \frac{2^m W_0(p_c^m - p_c^K)}{2(1 - p_c^K)} - \frac{1}{2} \right\}^{-1}. \quad (10)$$

Again, p_c is obtained as follows:

$$p_c = 1 - (1 - \tau)^{N_a - 1}, \quad (11)$$

where N_a is the number of active nodes. We can solve the system dynamics by solving independent Equations (10) and (11), and the existence of this solution is guaranteed by the fixed point theorem [15].

2) *Power distribution in a mutual sensing area*: Since we know τ , we can obtain the steady state power density. The probability that i nodes transmit simultaneously at an arbitrary time slot, given that N_a transmitting nodes are deployed in a mutual sensing area, is computed as follows:

$$p_a(m) = \mathbb{P}[i = m | N_a = a] = \binom{a}{m} \tau^m (1 - \tau)^{a-m} \quad m = 0, \dots, a. \quad (12)$$

Each transmitting node's operation in a mutual sensing area is synchronized, since the medium is sensed perfectly and every node uses the inner clock. Idle time is segmented into multiple slot times (σ). All events (idle time slots, successful and collision time slots) can be distinguished by their own time lengths. At an arbitrary time slot called the *virtual time slot*, the medium in the mutual sensing area is in one of three events, and the virtual time slot has the random duration T_v . We assume that the payload size is PAY for all nodes. In the basic mode,

$$T_v = \begin{cases} \sigma, & \text{for the idle slot time,} \\ T_s^{BAS} (= PHY + \lceil \frac{MAC+PAY}{R_s} \rceil T_s + SIFS + ACK + DIFS), & \text{for the successful slot time,} \\ T_c^{BAS} (= PHY + \lceil \frac{MAC+PAY}{R_s} \rceil T_s + DIFS), & \text{for the collision slot time,} \end{cases}$$

where PHY , $SIFS$, ACK , and $DIFS$ are the durations of the PHY header, SIFS (short interframe space) time, ACK packet, and DIFS (DCF interframe space) time, respectively. MAC , R_s and T_s are the MAC header size, symbol rate and symbol duration, respectively. Besides, superscript BAS denotes the basic mode and RTS denotes the RTS-CTS mode throughout the paper.

The transmissions of nodes are performed according to the following process. Once the transmission starts, a packet of size $PHY + \lceil \frac{MAC+PAY}{R_s} \rceil T_s$ is transmitted first. Then the remaining parts ($SIFS + ACK + DIFS$ or $DIFS$) are transmitted only if a collision has not happened. In RTS-CTS mode, an additional interval is needed for RTS-CTS transmission, and the times are changed to $T_s^{RTS} (= RTS + CTS + PHY + \lceil \frac{MAC+PAY}{R_s} \rceil T_s + 3 * SIFS + ACK + DIFS)$ and $T_c^{RTS} (= RTS + DIFS)$ respectively. RTS and CTS are the durations of the RTS and CTS packets, respectively.

T_v has the PMF induced from (12) such as $p_a(0)$, $p_a(1)$, and $1 - p_a(0) - p_a(1)$, which are for idle, successful transmission, and collision events, respectively. We derive the mean virtual time slot, $\mathbb{E}[T_v]$, using this PMF for each mode.

$$\begin{aligned} \mathbb{E}[T_v^{BAS}] &= \sigma p_a(0) + T_s^{BAS} p_a(1) + T_c^{BAS} (1 - p_a(0) - p_a(1)), \\ \mathbb{E}[T_v^{RTS}] &= \sigma p_a(0) + T_s^{RTS} p_a(1) + T_c^{RTS} (1 - p_a(0) - p_a(1)). \end{aligned}$$

The distribution of the number of concurrent transmissions (which is also the power distribution) is based on this PMF. In each virtual time slot, the number of concurrent transmissions varies from 0 to N_a because it is possible that nobody transmits in a certain virtual time slot, even if there are some active nodes in the mutual sensing area. In the basic mode, nobody transmits during σ . During $SIFS$ and $DIFS$ in both the successful and collision slot times, nobody transmits. During the packet transmission

$$B_a^{BAS}(j) = \frac{1}{\mathbb{E}[T_v^{BAS}]} \cdot \begin{cases} \sigma p_a(0) + (SIFS + DIFS)p_a(1) + DIFS(1 - p_a(0) - p_a(1)), & j = 0 \\ (PHY + \lceil \frac{MAC+PAY}{R_s} \rceil T_s + ACK)p_a(1), & j = 1 \\ (PHY + \lceil \frac{MAC+PAY}{R_s} \rceil T_s)p_a(j), & 2 \leq j \leq a. \end{cases} \quad (13)$$

$$B_a^{RTS}(j) = \frac{1}{\mathbb{E}[T_v^{RTS}]} \cdot \begin{cases} \sigma p_a(0) + (3SIFS + DIFS)p_a(1) + DIFS(1 - p_a(0) - p_a(1)), & j = 0 \\ (RTS + CTS + PHY + \lceil \frac{MAC+PAY}{R_s} \rceil T_s + ACK)p_a(1), & j = 1 \\ RTS \cdot p_a(j), & 2 \leq j \leq a. \end{cases} \quad (14)$$

time $(PHY + \lceil \frac{MAC+PAY}{R_s} \rceil T_s$ and ACK) in a successful slot, one node transmits, while multiple nodes transmit during $PHY + \lceil \frac{MAC+PAY}{R_s} \rceil T_s$ in a collision slot. In the RTS-CTS mode, the power density is changed in the same manner. Therefore, the actual power distribution, $\mathbb{P}[j \text{ nodes transmit} | N_a = a]$ is obtained using this distribution in the basic mode (Equation (13)) and RTS mode (Equation (14)). The probability of a busy channel in a mutual sensing area p_{on} is $\sum_{j=1}^a B_a^{BAS/RTS}(j) = 1 - B_a^{BAS/RTS}(0)$.

D. Effective active node density

So far, we have introduced a mutual sensing area using the spatial boundary of the Boolean CS operation, and have derived the distribution of the number of nodes, which is $\mathbb{P}[N = n]$ as in Equation (7) in Section III-A. We derived the probability of the number of active nodes for a given number of users in the mutual sensing area, $\mathbb{P}[N_a = a | N = n]$ as in Equation (8) in Section III-B. As seen from (9), the results are all based on the value of p_{on} , the probability that the mutual sensing area is busy. We can get the value of p_{on} by finding the intersection of the right and left hand sides of (18), which we will call p_{on}^* . Details of the derivation of p_{on}^* are given in Appendix II. Furthermore, the transmission probability of a node τ is derived in Section III-C1 to obtain p_{on}^* . Based on the transmission probability, the power distributions in the mutual sensing area can be calculated as in Equations (13) and (14) in Section III-C2.

If we obtain p_{on}^* , the distribution of the number of transmitting nodes in the mutual sensing area can be derived as in (17), where the number of actual transmitting nodes (active and non-frozen) in the area is denoted by Z . The expected number of transmitting nodes is derived from this result:

$$\mathbb{E}[Z] = \sum_{z=0}^{\infty} z \cdot \mathbb{P}[Z = z] \quad (15)$$

The effective active node density is defined as the average number of transmitting nodes per unit area. Thus, we finally obtain the effective active node density as follows:

$$\mathbb{P}[Z = z] = \sum_{n=z}^{\infty} \left(\frac{\{\lambda\pi(\frac{R}{2})^2\}^n}{n!} e^{-\lambda\pi(\frac{R}{2})^2} \sum_{a=z}^n \mathbb{P}[N_a = a|N = n] \right) B_a(z), \text{ for } z \in \{0, 1, \dots\} \quad (17)$$

$$\begin{aligned} p_{on} &= \sum_{n,a} \sum_{j=1}^a B_a(j) = \sum_{n=0}^{\infty} \mathbb{P}[N = n] \sum_{a=0}^n \mathbb{P}[N_a = a|N = n] \sum_{j=1}^a B_a(j) \\ &\stackrel{(a)}{=} \sum_{n=1}^{\infty} \mathbb{P}[N = n] \sum_{a=1}^n \mathbb{P}[N_a = a|N = n] \sum_{j=1}^a B_a(j) \\ &\stackrel{(b)}{=} \sum_{n=1}^{\infty} \frac{\{\lambda\pi(\frac{R}{2})^2\}^n}{n!} e^{-\lambda\pi(\frac{R}{2})^2} \sum_{a=1}^n \sum_{\eta} P_{n,a,\eta} p_{\eta} \sum_{j=1}^a B_a(j) \\ &\stackrel{(c)}{=} \sum_{n=1}^{\infty} \frac{\{\lambda\pi(\frac{R}{2})^2\}^n}{n!} e^{-\lambda\pi(\frac{R}{2})^2} \sum_{a=1}^n \sum_{\eta} P_{n,a,\eta} \left\{ \sum_D O_{\eta}^D p_{on}^D (1 - p_{on})^{8-D} \right\} \sum_{j=1}^a B_a(j) \end{aligned} \quad (18)$$

$$\lambda' = \frac{\mathbb{E}[Z]}{\pi(\frac{R}{2})^2}. \quad (16)$$

This is used in the cumulative distribution function (CDF) (1) and the probability density function (PDF) (2) of the aggregate interference. We plot the resulting CDF and PDF for varying network parameters and compare these with the simulation results in Section IV.

IV. VERIFICATION OF THE ANALYSIS

In this section, we plot the effective node density (λ') of (16), and the CDF (1) and PDF (2) of the aggregate interference using λ' . Next, we compare the derived results with those obtained in the NS-2 and Matlab simulations. For all of the simulation scenarios, the exclusion radius r in the dependent processes is given as 70m. In the NS-2 simulation, the MAC/PHY parameters and channel model are given so that the CS radius R is determined to be 50, 70 and 100 (m). The purpose of this Matlab experiment is to investigate the MHC and SSI, which are the dependent processes reflecting the ideal CSMA networks. The NS-2 simulation, on the other hand, evaluates the practical CSMA/CA network case. By doing these two simulations, we can show i) the difference between the MHC and SSI processes, and ii) the difference between practical CSMA/CA networks and ideal CSMA networks. These results are shown in Figs. 7 and 8. Using Matlab, we only evaluate the aggregate interference of the ideal CSMA (not practical CSMA/CA) network, where the CS operation is done deterministically at every node and there are no time dynamics in the networks. In NS-2, all possible practical operations of the 802.11 DCF protocols are implemented

TABLE I
SIMULATION PARAMETERS FOR MHC AND SSI PROCESSES.

Fixed Parameters	
Transmission power (p)	0.001(W)
Background Plane	Circle ($B(O, R)$)
Radius of Background Plane ($R_M = R_S$)	282 (m)
Exclusion Ball Radius (r)	70 (m)
Number of Iterations (n)	100000
Channel Model	$\frac{X}{d^4}$, where $X \sim \text{Exp}(1/p)$
Varying Parameters	
Node Density (λ)	$\{1, 2, 3, 4, 5\} * 10^{-4}$

and simulated. Therefore, the CS operation is done at every sending node and channel fading/attenuation is considered. In NS-2 experiments, the active node topology dynamically changes over the time slots for one given initial node deployment, and we average the aggregate interference for this varying active node topology. The initial node deployments are repeated randomly for both the Matlab and NS-2 simulations.

A. Simulation setup

1) *MATLAB simulation for MHC and SSI*: We deployed the points using the MHC and SSI processes, as explained in [12], with MATLAB. The parameters used in the simulations are listed in Table I¹. For a given number of nodes, the aggregated power was measured at O , which is the center of ball B with radius R_M or R_S for MHC or SSI, respectively. The number of deployed nodes was generated using a Poisson distribution with the parameter $\lambda|B|$, where λ is the initial node density and $|B|$ is the area of ball B . We deployed these points uniformly and measured the aggregate power at O . We repeated this procedure for more than 100,000 iterations.

2) *NS-2 simulation for PPP*: To verify the analysis results, we conducted simulations using NS-2 [16], which includes wireless PHY and MAC layer patches for the realistic IEEE 802.11 DCF standard [17]. This enabled us to realistically simulate the PHY and MAC stacks of the IEEE 802.11 DCF. The simulation parameters, which are the defaults for IEEE 802.11a PHY and MAC and are from the previous research [18], are listed in Table II.

The overall simulation procedure consist of NS-2 simulations, pre-processing of the scenario, and post-processing of the data. In the pre-processing stage, the number of transmitting nodes is generated using the Poisson distribution, the nodes are deployed uniformly, the designated receiving nodes are

¹Refer to [12] for the meanings of parameters and details of the process.

attached to each transmitting node, and traffic is generated for each transmitting node. For the saturated traffic situation, we obtained the time duration from $\max_i\{\text{the first transmission time of node } i\}$ to $\min_i\{\text{the last transmission time of node } i\}$. We call this the time window. The post-processing stage consists of finding the time window, measuring the received power at the measuring node, recording the duration of each received power value, and accumulating all of the measurements.

In attaching the receivers to transmitters, we fixed the relative location of each receiver at 5m to the right and 5m above its transmitter. To measure the aggregate power, we put the measuring node in the center of the simulation grid. This node then reports the received power level, and we record the duration and power level of each received signal.

The simulation conducted in this paper is full-scaled, which takes a long time to collect meaningful results for two reasons. First, each simulation per geometry scenario takes a long time, including the simulation time of NS-2 and the post-processing time for handling the received power instances. NS-2 traces all of the packet-level transactions with the received power recorded at every receiver. In the post-processing stage, the calculation of the received power from all of the ongoing transmissions at a measuring node takes computation time. Moreover, the simulation time itself (not the computation time) has to be long enough to reflect the steady-state behavior, which theoretically requires infinite investigation time. We consider at least 30 seconds per scenario as the simulation time (this takes about 2 hours in real time using a Quad core i7 processor computer). Second, to get a sound statistical inference of PPP, we repeat the per-geometry simulation 50 times since all of the resulting PDFs of the aggregate interference obtained from the simulations converge before 30 repetitions. The simulation time for all 50 scenarios takes approximately four days on average. We repeat this process for each combination of the PHY and MAC layer parameters.

Saturated traffic was assigned to all transmitters so that there was no idle time by the traffic itself during the simulations. The background grid for all of the simulation scenarios was always a 500m by 500m square. The transmission times for RTS, CTS, PPDU (PHY+MAC+PAY) with 500 B (or 1000 B) of payload and ACK were 52, 44, 728 (or 1396), and 44 (μs), respectively (see Table II and [18]). We ignored the propagation delay, even though this exists in the simulator, because the value was quite small compared to the other transmission times. Generated traffic of 5,000,000 packets per second (pps) was given to all of the transmitters. This means a value of 0.2 (μs) for the inter-arrival time from the application layer to the physical layer, which is less than the whole transmission time for one successful

TABLE II
SIMULATION PARAMETERS FOR NS-2.

Fixed Parameters	
Background Grid	Regular Rectangular
Grid Size	500(m)*500(m)
Transmission power	0.001(W)
Initial window size W_0	16
Maximum backoff stage m	6
CW min/max	15/1023
Slot Time (σ)	9(us)
SIFS	16(us)
DIFS	SIFS+2 σ =34 (us)
Short Retry Limit K	7
Long Retry Limit K	4
PLCP Preamble Duration	16 (us)
PLCP Header duration except Service field	20(us)
OFDM Symbol Duration	4(us)
IFQ Length	50
RTS MPDU + Service + Tail Field	182(bits)
CTS MPDU + Service + Tail Field	134(bits)
ACK MPDU + Service + Tail Field	134(bits)
Data Rate	6(Mbps)
Control Rate	1(Mbps)
Modulation	BPSK
Code Rate	1/2
Carrier Frequency	5.18 (GHz)
Preamble Capture Threshold	2.5118
Data Capture Threshold	100
Noise Floor	10^{-12} (W)
Data Type	CBR
CBR Rate	$5 * 10^6$ (packets per sec)
Number of Packets in the application queue	3000
Channel Model	$\frac{X}{d^4}$, where $X \sim \text{Exp}(1/p)$
Varying Parameters	
Payload Size	500 or 1000 (Bytes)
RTS Threshold	0 or 10000
Node Density (λ)	$\{1, 2, 3, 4, 5\} * 10^{-4}$
Effective CS Range (R)	50, 70, 100(m)

packet, i.e., $RTS + CTS + PHY + MAC + PAY + ACK + 3 * SIFS + DIFS = 948(\mu s)$. The inter-arrival time is enough for the traffic to be saturated.

B. Discussions

1) *Analysis results of p_{on} and λ'* : p_{on} in this subsection refers to p_{on}^* , which can be found from (18), and is the final solution of p_{on} for simplicity of expression. In Fig. 3, the values of p_{on} are shown for various

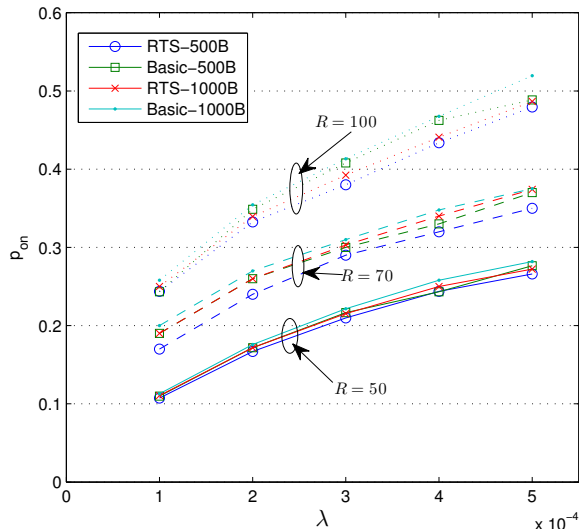


Fig. 3. P_{on} versus λ for all combinations of MAC layer parameters.

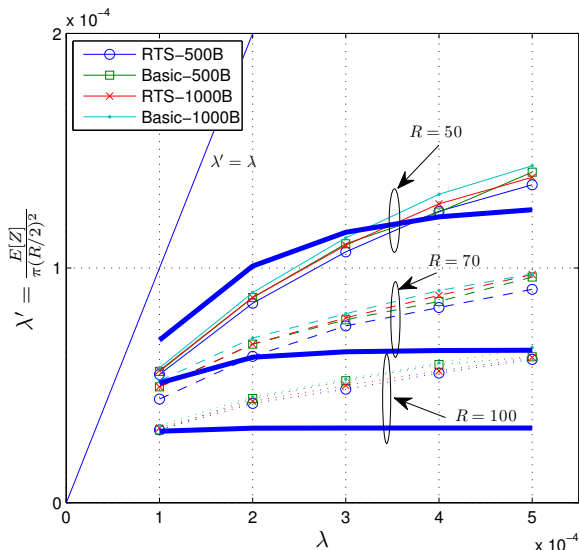


Fig. 4. New node density λ' for initial node density λ and MAC layer parameter combinations. The thicker curves are using λ' in (19).

combinations of MAC parameters. The factor that affects p_{on} the most is the effective CS distance R , followed by λ , which is the initial node density. As λ increases, p_{on} naturally increases due to the increased congestion level with the log shape. If there is only the reduced idle time factor without increasing the collision probability, as in [14]'s ideal CSMA, the rate of increase of p_{on} must be a log function. However, our model reflects the increased collision probability and reduced idle time simultaneously, as obtained in real situations. The resulting p_{on} shows a mixture of linear and log functions. Within the same R , the combination of mode and payload size that has the lowest p_{on} is the RTS mode and short payload. In other words, the order of $\{RTS - 500B, Basic - 500B, RTS - 1000B, Basic - 1000B\}$ is for lower

p_{on} . In general, RTS-CTS mode has a lower congestion level than the basic mode since the only system cost was the RTS-CTS packet collision and the waiting time for retransmission as compared to the basic mode. A large payload in the basic mode makes for a higher congestion level. However, in the cases of some λ values, RTS-CTS packets were small enough to compensate for the payload size. Therefore Basic-500B might have higher values of p_{on} than RTS-1000B. In this case, the effect of the mode was weaker than that of the payload size.

This p_{on} was used in the new density λ' (16) and we plotted this as shown in Fig. 4. This figure shows that the smaller R makes for a higher λ' , which is the opposite of p_{on} . This is understandable, since a smaller R signifies more insensitivity to the interference. Therefore, we expected the result of $R = 0$, the ALOHA system, to approach the line $\lambda' = \lambda$ in the figure. This line also represents wireless access systems that have no MAC, such as macro or femto cellular systems. The curve λ' is a version of λ filtered by the CSMA/CA and BEB mechanism. By showing the $\lambda' = \lambda$ line and the curves together, Fig. 4 also addresses the size of the gap between the original node density and effective node density and the effectiveness of CSMA/CA MAC. The bold curves are from:

$$\lambda'' = \frac{1 - \exp(-\lambda\pi D^2)}{\pi D^2} \quad (19)$$

where D is the exclusion distance. For comparison, we put R into D in this figure. This expression is the approximated node density for modeling the MHC adopted in [10] and [19]. As shown in the figure, the variation of λ' is higher than that of λ'' for varying λ . Since λ'' is used for modeling dependent point processes, it cannot trace the real operation. As shown in the next section, our aggregate power distribution adopting λ' is the most accurate among the other point processes. Therefore, Fig. 4 shows the gap in the aggregate interference between simplified MHC and the real situation. This is significant because this simplified MHC expression is widely used in academia [10], [11], [19], [5].

2) *Comparison of the resulting aggregate interference with the simulation:* Using this λ' and the shot noise analysis, we plotted the distribution of the aggregate interference. The PDF and CDF of the analysis in each node density showed high correlations with those of the NS-2 simulations as seen in Figs. 5 and 6. We depict all of the PDFs in a log scale. Although at first glance they resemble a log-normal distribution, they are asymmetric based on the main lobe.

Therefore, they are definitely neither normal nor log-normal distributions. This is notable as some research efforts in the signal processing field assume that the aggregate interference follows normal (in

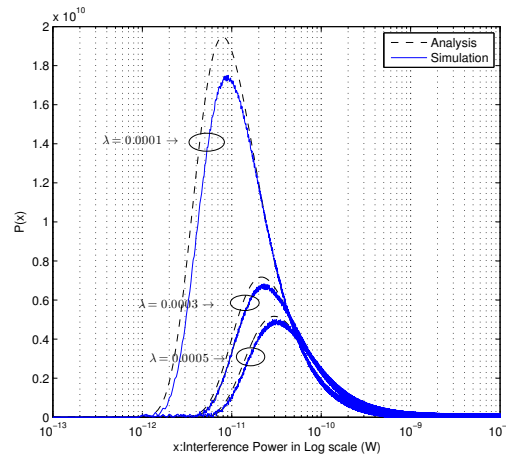


Fig. 5. Probability density of aggregate interference in the condition of RTS mode, 500B payload and $R = 70(m)$. Other parameters are in Table III.

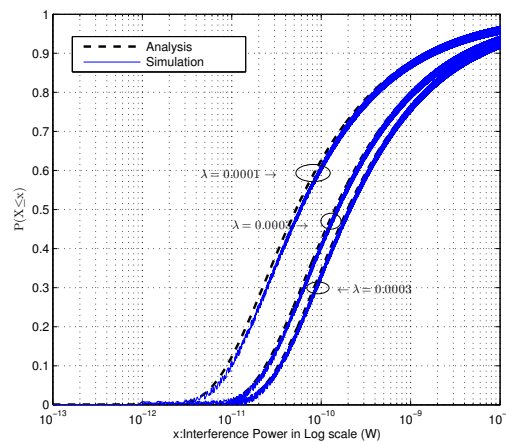


Fig. 6. Cumulative distribution of aggregate interference in the condition of RTS mode, 500B payload and $R = 70(m)$.

dBm unit) or log-normal (in W unit) distributions. For the other features, the higher the mean of the aggregate power, the lower the probability of that mean value. Therefore, low-mean high-probability and high-mean low-probability patterns are shown in all of the results. This is because the total sum of the probability is fixed at 1 and the x-axis is log-scaled and not linear.

Compared with dependent point processes, at any given λ value, our analysis is the closest one to the simulation results, as depicted in Fig. 7 and Fig. 8. The interference of MHC is always less than that of SSI since MHC is the lower bound of SSI, which is also commented on in [12]. However, these two are not as sensitive as our model to variations in the node density. Moreover, these two do not have sufficient MAC and PHY layer parameters to reflect the real situation, while our analysis can model any combination of the system parameters, as in Fig. 9.

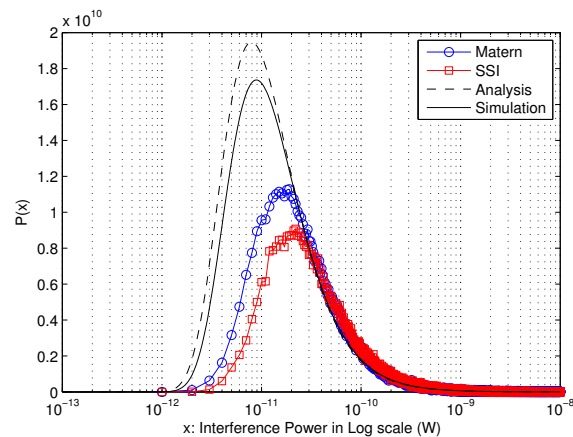


Fig. 7. Probability density of aggregate interference when λ is 0.0001.

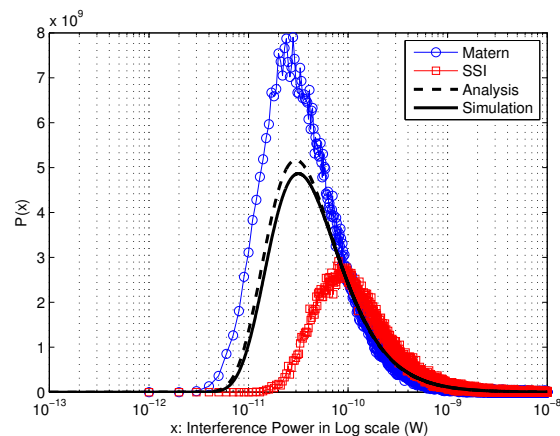


Fig. 8. Probability density of aggregate interference when λ is 0.0005.

As shown in the figures so far, our model of the aggregate interference has slightly lower values than that of the simulation in each case. This is mainly because the simulator allows the *capture* situation. In our analysis, a collision between transmitters is regarded as a failure of transmission, and this increases each collided node's backoff stage. In contrast, there might be a successful transmission even when multiple nodes in a CS area are transmitting at the same time. This is because if the ratio of one incoming signal to the others is guaranteed to be higher than a certain threshold, the stronger incoming signal can always be decoded². In our analysis, we ignored that situation in order to simplify the analysis. Nevertheless, our result is valid.

From these results, we learned the following lessons: If the network is required to maintain a lower interference than a certain level, there are multiple combinations of parameters that need to be controlled. Since the PDF of the aggregate interference is a function of λ' , there are multiple combinations of

²The patch in NS-2 has two capture thresholds: the preamble capture and the data capture. Thus, these two capture events can also occur in the simulations.

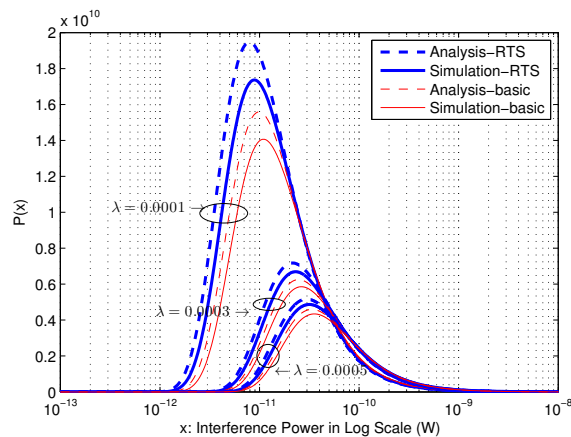


Fig. 9. Probability density of aggregate interference in the case of 500B payload and $R = 70$.

parameters that can result in the same value of λ' . Those controllable parameters are R , the transmission mode, payload size, etc. This can be used for the interference management in uncontrolled interference limited systems such as cognitive radio networks.

V. CONCLUSION

In this paper, we analyzed the aggregate interference from randomly deployed CSMA/CA nodes. Due to the imperfection of the CSMA/CA protocol, the transmission of each node in the network is not fully dependent, but is independent of the new node density. The effective node density reflecting this characteristic is derived by spatially quantizing the infinite space and analyzing the steady-state power distribution of this quantization unit.

Our framework derived to find this value reveals the relation of the MAC parameters and the effective node density. Although the exact closed form expression of the interference distribution cannot be obtained, the sound simulation using NS-2 certifies that the analysis is enough to be used for optimizing the system parameters in uncontrolled WiFi hot spots or to protect incumbent systems in the case of secondary spectrum access.

APPENDIX I: DERIVATION OF $\mathbb{P}[N_a = a | N = n]$

The following proposition gives the grounds for splitting a typical residual sensing area.

Proposition 1. Each residual sensing area can be thought of as the union of three independent, equally sized and mutually disjoint areas, and the size of this area is the same as $|H|$.

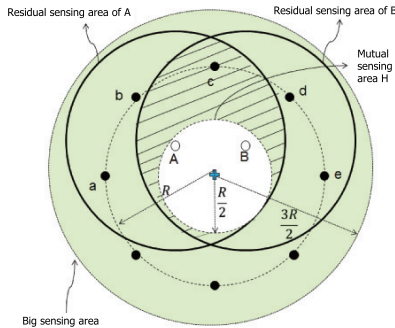


Fig. 10. *Residual sensing areas of multiple nodes of a mutual sensing area.* There are two nodes $\{A, B\}$ in a mutual sensing area. Residual sensing areas of two nodes include three black dots, $\{a, b, c\}$ and $\{c, d, e\}$ respectively. The hashed region is overlapped by both the residual sensing areas of nodes A and B . A dot (c) is included in this overlapped region, and means the quantized space occupied by this region.

Proof. Given the homogeneity of PPP, i.e., the point process is characterized by the area of the space not by the location or shape, where the size of the residual sensing area is $\frac{3\pi R^2}{4}$, which is three times that of the mutual sensing area. Therefore, if we measure the residual sensing area and compare it with the size of the mutual sensing area, we find that three mutual sensing areas constitute one residual sensing area.

■

According to **Proposition 1**, for one of the sensing nodes in H to be an active node, there should not be any transmission in any of these three independent areas with area $|H|$. Since the point deployment is only specified by the size of the space, the probability that a node in H is an active node is a function of the activity in three subspaces. From this, the probability is

$$(1 - p_{on})^3. \quad (20)$$

However, if multiple nodes are deployed in H , their CS operations are not independent of each sensing node since the residual sensing area of each node must partially overlap, as in Fig. 10.

Due to this partial dependence of CS among multiple sensing nodes, the probability that a node in H is an active node is not straightforward like (20) and the exact dependent CS probability cannot be derived. To the best of our knowledge, even state-of-the-art research on stochastic geometry cannot reveal the exact distribution on the overlapped area when circles are deployed by PPP. Therefore, we use a spatial quantization approximation, in which some evenly distributed dots are the measure of the overlapped residual sensing area.

We use eight dots that are evenly distributed in terms of the angle as shown in Fig. 10. The number of dots included in the intersection of any residual sensing areas denotes the corresponding overlapped

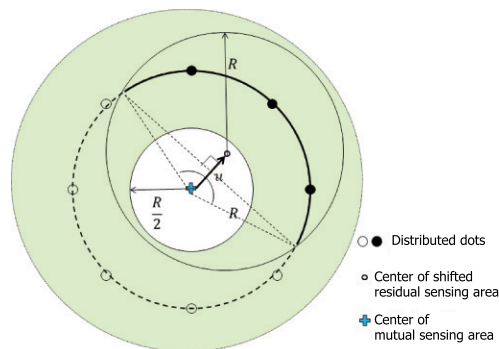


Fig. 11. Each residual sensing area includes 3 consecutive dots in the *big sensing area*. Each dot represents one of three sensing areas.

area in the unit of H . Furthermore, each dot is “on” with p_{on} and indicates whether or not there is an ongoing transmission in the corresponding overlapped area.

Now, we introduce a large circle with radius $\frac{3R}{2}$ that can cover the residual sensing areas of all possible nodes in H . We call this circle a *big sensing area*. There are eight dots in the large sensing area. They are evenly distributed in terms of the angle. As depicted in Fig. 11, any sensing node in H includes three dots, except for the case in which the sensing node is located exactly at the center of H .

Proposition 2. When eight dots are evenly distributed on the circumference of a circle of radius R , the residual sensing area of any sensing node in H covers three consecutive dots.

Proof. Let vector u characterize the shifting of the residual sensing area from the center of the large sensing area to a random position. The circumference of the original residual sensing area partially overlaps the shifted one. This partial circumference (the thick segment of the line in Fig. 11) has an angle measured at the center of the mutual sensing area, which is $2\cos^{-1}(\frac{|u|}{R})$. Since $0 < |u| \leq \frac{R}{2}$ by the definition of u , the angle derived from u is bounded in the interval $(\frac{\pi}{3}, \pi]$. This angle always includes three consecutive dots. ■

We measure the overlapped residual sensing area using these dots. Each dot is “on” with p_{on} and “off” with $1 - p_{on}$, where p_{on} for all dots is the same and the on-off Booleans are independent of each other. Also, the on-off Boolean indication of each dot denotes the existence of an ongoing transmission, and the number of dots in the intersection of the residual sensing areas denotes the area of the corresponding overlapped area. The residual sensing area of any node in the mutual sensing area can be mapped into one of three-consecutive-dots according to **Proposition 2**.

Conversely, the possible region of a sensing node having the same three-consecutive-dots exists in H

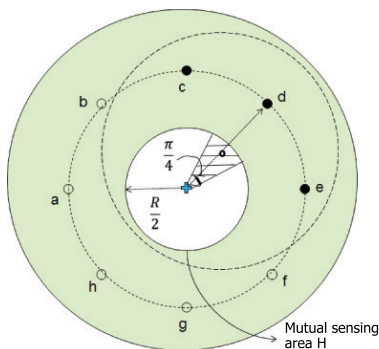


Fig. 12. The hashed region is the possible region of a sensing node having three-consecutive-dots $\{c, d, e\}$. This area has an angle of $\frac{\pi}{4}$ which is split evenly by the direction to the center dot of $\{c, d, e\}$. If $\{c, d, e\}$ are all ‘off’, this $\{c, d, e\}$ becomes *three-offs*. The number of three-offs is bounded in $[0, 8]$ in H .

as in Fig. 12. All sensing nodes located in this region follow the same CS result, i.e., on-off. For example, three consecutive ‘off’ dots mean that the residual sensing area containing these dots does not have any transmissions in its area, and the corresponding sensing node is *active*. In contrast, if there is at least one ‘on’ dot among the three, this means that the corresponding sensing node is *inactive*.

Any random position of a sensing node in H can be mapped into one of eight three-consecutive-dots, and the probability of each dot being on is p_{on} . Therefore, the problem of finding active nodes given N initially deployed nodes in H is solved in two stages. The first stage is to examine the case in which three-consecutive-dots are all in “off” states where the on-off behaviors of the dots are independent. The second stage is to determine how many of the three-consecutive-dots in the “off” state (simply say ‘*three-offs*’) are picked up through N independent choices. The number of all possible sequences of eight binary digits (representing the on-off states of a dot) are $2^8 = 256$. By counting all combinations of these digits, we derive the PMF of the number of three-offs. Let us denote the number of three-offs by η . For the values of $\eta = \{0, 1, 2, 3, 4, 5, 6, 7, 8\}$, the number of occurrences of each η is $\{131, 56, 36, 16, 8, 8, 0, 0, 1\}$, respectively. These numbers are obtained simply by counting consecutive three-offs in all combinations of eight binary digits (or dots), as shown in Fig. 13.

These occurrences are also categorized according to the number of “on” dots among eight dots, which is denoted by D . By counting each combination, we obtain the quantity O_η^D , which represents the number of times that D out of eight are “on” dots when there are η three-offs, as in Table III.

Therefore, the probability that there are η three-offs given p_{on} is:

$$p_\eta = \mathbb{P}[\eta \text{ three-offs}] = \sum_{D=0}^8 O_\eta^D p_{on}^D (1 - p_{on})^{8-D}.$$

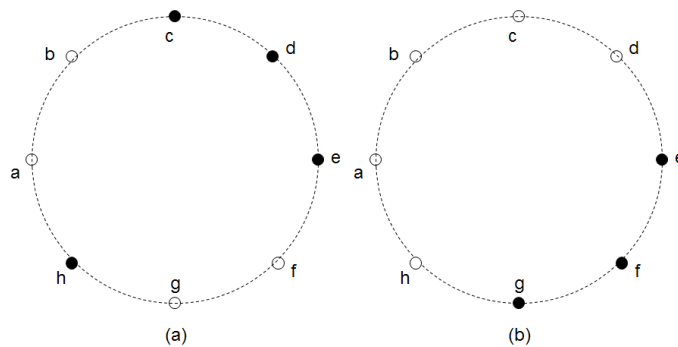


Fig. 13. Example of counting three-offs. If the solid dot means ‘off’, $\eta = 1$ in both cases, while $D = 4$ and 5 in (a) and (b) respectively. By counting all on-off combinations, we obtain Table III.

TABLE III
 O_η^D

η	D									Sum(η)
	0	1	2	3	4	5	6	7	8	
0	0	0	0	8	38	48	28	8	1	131
1	0	0	0	24	24	8	0	0	0	56
2	0	0	12	16	8	0	0	0	0	36
3	0	0	8	8	0	0	0	0	0	16
4	0	0	8	0	0	0	0	0	0	8
5	0	8	0	0	0	0	0	0	0	8
6	0	0	0	0	0	0	0	0	0	0
7	0	0	0	0	0	0	0	0	0	0
8	1	0	0	0	0	0	0	0	0	1
Total	1	8	28	56	60	56	28	8	1	256

Once p_{on} is given, p_η is determined using this equation. Since uniformly deployed sensing nodes in H have any three consecutive dots according to **Proposition 2**, the probability of becoming an active node is equal to the probability that the residual sensing area of that sensing node has one of η three-offs. Therefore, the probability that a sensing node uniformly deployed in H becomes an active node is $\frac{\eta}{8}$ ($\eta = 0, 1, \dots, 8$). A sensing node is located in H uniformly and independently. Hence, if there are n sensing nodes in H , the event that a out of n sensing nodes become active nodes is equal to the Bernoulli process with the parameter $\frac{\eta}{8}$. Then, $N_a \sim B(n, \frac{\eta}{8})$. Let us define $P_{n,a,\eta}$ as the probability that a out of n sensing nodes have one of η three-offs when η is given. Then,

$$P_{n,a,\eta} = \mathbb{P}[N_a = a|n, \eta] = \binom{n}{a} \left(\frac{\eta}{8}\right)^a \left(1 - \frac{\eta}{8}\right)^{n-a}.$$

Finally, N_a is bounded in $[0, N]$, and the conditional probability that $N_a = a$ given $N = n$ is:

$$\mathbb{P}[N_a = a|N = n] = \sum_{\eta=0}^8 P_{n,a,\eta} p_\eta,$$

$$a = 0, \dots, n.$$

APPENDIX II: DERIVATION OF p_{on}

The power distributions $B_a(j)$ of (13) and (14) are conditioned on N_a , while N_a is conditioned on N . Therefore, the marginal PMF of p_{on} is obtained by summing all of the probabilities on conditioned variables, as in (18). The condition on N_a is eliminated using (8). The condition on N is eliminated by the homogeneity of PPP, i.e., every geometric subset satisfies the Poisson distribution of the number of points in that subset, i.e., (7).

In (18), part (a) is from the fact that the possibility of a mutual sensing area being “on” is zero when there are no initial deployed nodes and active nodes. Part (b) is from Equations (7) and (8). Part (c) is from Equation (9). In this equation, p_η includes the p_{on} term, which is also the marginal PMF from the unconditional event of channel busyness. Therefore, Equation (18) has the unknown variable p_{on} on both sides of the equation, and the solution can be obtained by solving the weighted eighth order polynomial of p_{on} , where the weight is the product form of the Poisson and binomial probabilities. More specifically, $\sum_{a=1}^n \sum_{\eta} P_{n,a,\eta} \{ \sum_D O_\eta^D p_{on}^D (1 - p_{on})^{8-D} \} \sum_{j=1}^a B_a(j)$ is the eighth-order polynomial of the unknown p_{on} and all other terms are known, and $\frac{\{\lambda\pi(\frac{R}{2})^2\}^n}{n!} e^{-\lambda\pi(\frac{R}{2})^2}$ is a constant from the Poisson distribution for the given n . Therefore, summing the product of these two terms for varying n from $n = 1$ to $n = \infty$ also results in an eighth-order polynomial. Since there is no general solution for polynomials with an order higher than four and n goes to infinity, we cannot derive the closed form expression of p_{on}^* , the solution of p_{on} . However, we can still get a solution by finding the intersection of the right hand side and left hand side of (18), which we call p_{on}^* .

REFERENCES

- [1] 3GPP TR 36.889 v0.3.1, “Study on Licensed-Assisted Access to Unlicensed Spectrum,” February 2015.
- [2] M. Tercero, K. W. Sung, and J. Zander, “Impact of aggregate interference on meteorological radar from secondary users,” *Proc. IEEE WCNC*, 2011.
- [3] K. Koufos, K. Ruttik, R. Jantti, “Aggregate interference from WLAN in the TV white space by using terrain-based channel model,” *Proc. CROWNCOM*, 2012.
- [4] F. Baccelli, and B. Błaszczyszyn, “Stochastic geometry and wireless networks volume 1: theory,” *Foundations and Trends in Networking*, Vol. 3, No. 3-4, pp. 249-449. 2009.

- [5] M. Haenggi, and R. K. Ganti, "Interference in large wireless networks," *Foundations and Trends in Networking*, Vol. 3, No. 2, pp. 127-248 2009.
- [6] D. M. Kim and S.-L. Kim, "An Iterative Algorithm for Optimal Carrier Sensing Threshold in Random CSMA/CA Wireless Networks," *IEEE Comm. Letters*, Vol. 17, No. 11, pp.2076-2079, 2013.
- [7] J. Hwang, and S.-L. Kim, "Cross-layer optimization and network coding in CSMA/CA-based wireless multihop networks," *IEEE/ACM Trans. on Networking*, Vol. 19, No. 4, pp. 1028-1042, 2011.
- [8] A. Hasan, and J. G. Andrews, "The Guard Zone in Wireless Ad hoc Networks," *IEEE Trans. on Wireless Comm.*, Vol. 6, No. 3, pp. 897-906, 2007.
- [9] Y. George and I. Bergel, "The Spectral Efficiency of Slotted CSMA Ad-Hoc Networks with Directional Antennas," *IEEE Trans. on Wireless Comm.*, Vol. 11, No. 10, pp. 3799-3809, 2012.
- [10] F. Baccelli, B. Blaszczyszyn, and P. Muhlethaler, "An ALOHA protocol for multihop mobile wireless networks, " *IEEE Trans. on Information Theory*, Vol. 52, No. 2, pp. 421-436, 2006.
- [11] J. Andrews, R. K. Ganti, M. Haenggi, N. Jindal, and S. Weber, "A primer on spatial modeling and analysis in wireless networks," *IEEE Comm. Magazine*, Vol. 48, No. 11, pp. 156-163, 2010.
- [12] A. Busson, G. Chelius, and J.-M. Gorce, "Interference modeling in CSMA multi-hop wireless networks," *Technical report INRIA*, inria-00316029-ver3, pp. 1-21, 2009.
- [13] H. ElSawy, and E. Hossain, "A Modified Hard Core Point Process for Analysis of Random CSMA Wireless Networks in General Fading Environments," *IEEE Trans. on Comm.*, Vol. 61, No. 4, pp. 1520-1534, 2013.
- [14] L. Jiang, and J. Walrand, "A distributed CSMA algorithm for throughput and utility maximization in wireless networks," *IEEE/ACM Trans. on Networking*, Vol. 18, No. 3, pp. 960-972, 2010.
- [15] G. Bianchi, "Performance analysis of the IEEE 802.11 distributed coordination function," *IEEE Journal of Sel. Areas on Comm.*, Vol. 18, No. 3, pp. 535-547. 2000.
- [16] Network Simulator-2 <http://isi.edu/nsnam/ns/>
- [17] Q. Chen, F. Schmidt-Eisenlohr, D. Jiang, M. Torrent-Moreno, L. Delgrossi, and H. Hartenstein, "Overhaul of IEEE 802.11 modeling and simulation in NS-2," *Proc. ACM MsWiM 07*, 2007
- [18] D. Qiao, S. Choi, and K. G. Shin, "Goodput analysis and link adaptation for IEEE 802.11a wireless LANs," *IEEE Trans. on Mobile Computing*, Vol. 1, No. 4, pp. 278-292, 2002.
- [19] D. Stoyan, W. S. Kendall, and J. Mecke, "Stochastic geometry and its applications," *John Wiley and Sons*, pp. 1-345, 1987.
- [20] R. Lawrence, "ALOHA Packet System With and Without Slots and Capture," *Computer Communications Review*, Vol. 5, No. 2, pp.28-42, 1975.